nature materials

SUPPLEMENTARY INFORMATION

DOI: 10.1038/NMAT4998

In the format provided by the authors and unedited.

Liquid Metal–Organic Frameworks

Romain Gaillac,[†,‡] Pluton Pullumbi,[‡] Kevin A. Beyer,[¶] Karena W. Chapman,[¶] David A. Keen,[§] Thomas D. Bennett,[*,‖] and François-Xavier Coudert[*,†]

†*Chimie ParisTech, PSL Research University, CNRS, Institut de Recherche de Chimie Paris, 75005 Paris, France*

‡*Air Liquide, Centre de Recherche Paris Saclay, 78354 Jouy-en-Josas, France*

¶*X-ray Science Division, Advanced Photon Source, Argonne National Laboratory, 9700 South Cass Avenue, Argonne, Illinois 60439, United States*

§*ISIS Facility, Rutherford Appleton Laboratory, Harwell Campus, Didcot, Oxon OX11 0QX, United Kingdom*

‖*Department of Materials Science and Metallurgy, University of Cambridge, 27 Charles Babbage Road, Cambridge CB3 0FS, United Kingdom*

E-mail: tdb35@cam.ac.uk; fx.coudert@chimie-paristech.fr

Supplementary Text

Microscopic mechanism

Characterization of the liquid ZIF

Supplementary Figures

Supplementary Figure 1: Experimental X-ray total pair distribution functions.

Supplementary Figure 2: Low-*r* region of the X-ray total pair distribution functions.

Supplementary Figure 3: Potential of mean force along the nitrogen–zinc distance coordinate

Supplementary Figure 4: Linear fit of the activation free energy.

Supplementary Figure 5: van 't Hoff plot of the number of defects.

Supplementary Figure 6: Frequency of Zn–N bond breaking.

Supplementary Figure 7: Frequency of Zn–Im bond breaking.

Supplementary Figure 8: van 't Hoff plot of Imidazolate diffusion coefficient.

Supplementary Figure 9: van 't Hoff plot of Zinc diffusion coefficient.

Supplementary Figure 10: Temperature evolution of the distribution of the accessible pore volume.

Supplementary Figure 11: Experimental and RMC X-ray structure factor data for the ZIF melt.

Supplementary Figure 12: Proportion of Zn^{2+} cations with four-fold coordination, as a function of temperature, for ZIF-4 and ZIF-8.

Supplementary Figure 13: Potential of mean force for ZIF-8, along the nitrogen–zinc distance coordinate, at different temperatures.

Supplementary Figure 14: Activation free energy for ZIF-8 as a function of temperature.

Supplementary Figure 15: Pore volume as a function of probe radius.

Supplementary Figure 16: X-ray structure factors upon heating.

Supplementary Tables

Supplementary Table 1: Thermodynamic properties values.

Supplementary Table 2: Characteristics of coordinative bond breaking.

Supplementary Table 3: Coordinative bond breaking dynamics.

Supplementary Table 4: Diffusion coefficients extracted from the MD simulations.

Supplementary Table 5: Summary of the densities used for RMC modeling and FPMD simulations.

Supplementary text: Microscopic mechanism

To shed light onto the microscopic mechanism of ZIF melting, we calculated the frequencies at which the Zn–N bonds or Zn–Im linkages break. Plotting the log of these frequencies against inverse temperature (see Figures S6 and S7) demonstrates the Arrhenian behaviour of the system, reinforcing the idea that melting is driven by rare events disturbing the network. We also note that the two activation energies for Zn–N and Zn–Im are very close. Extrapolating to the melting temperature — where in the limited time window of our simulations we cannot directly observe enough of these rare events to gather good statistics — shows that the timescale at which bond breaking occurs becomes sub-nanosecond near the melting temperature. As Table S2 shows, for any given zinc cation, we expect one coordinative bond breaking every 143 ms at 300 K, every 58 ns at 600 K, and every 0.87 ns at 840 K. Moreover, looking at these events in detail, we see that at low temperature, the majority of bond-breaking events leads to a simple flip of the imidazolate linker, and do not result in exchange between two linkers (Table S3). As temperature increases, this "local" motion of lower energy becomes dominated by events which lead to linker exchange, and thus allows the ZIF to melt. Finally, we see that the duration of the coordinative bond breaking and reformation is independent of temperature, and is only guided by the timescale for approach of another imidazolate partner and local dynamics.

Supplementary text: Characterization of the liquid ZIF

In addition to the characterization of translation diffusive behaviour (see main text), we find that the translational diffusion coefficients over temperature follow an Arrhenius law (see Figures S8 and S9), compatible with a jump-like diffusion of "partner exchange" events.[1] The activation energies for Zn and Im respectively are found to be 105 kJ.mol^{-1} and 102 kJ.mol^{-1} respectively. The rotational diffusion of imidazolate cycles can also be measured, where we choose to follow rotation around the N–N axis and the associated angle θ. Orientational diffusion happens at lower temperatures than translational diffusion, starting around 800 K, and can be associated with an activation energy three times lower ($\approx$ 40 kJ.mol^{-1}). At intermediate temperatures, before melting, there thus exists a regime of free rotation of the imidazolate linkers.

[1] Laage, D.; Hynes, J. T. On the Molecular Mechanism of Water Reorientation. *J. Phys. Chem. B* **2008**, *112*, 14230–14242

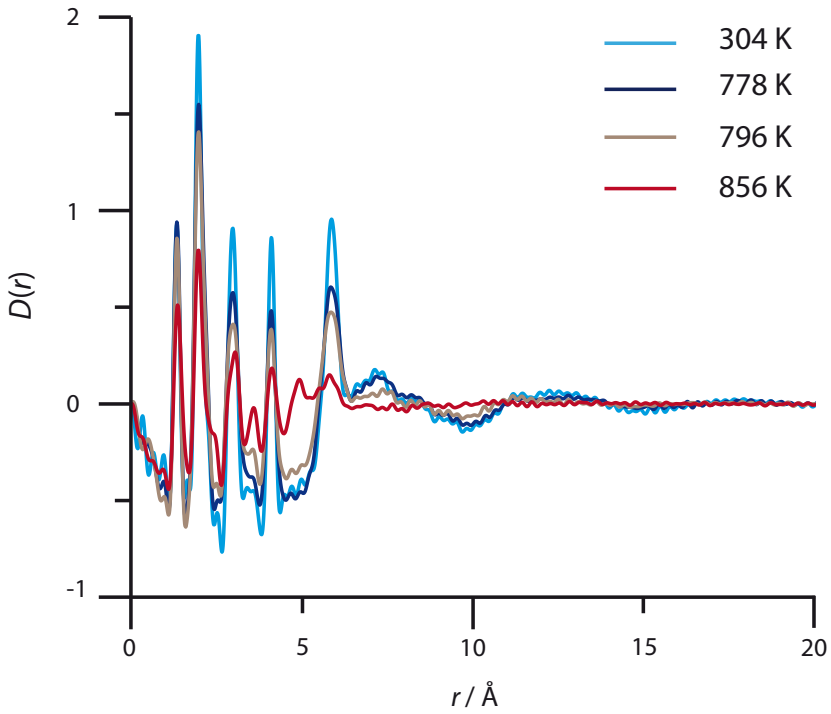

Supplementary Figure 1. Experimental X-ray total pair distribution functions at different temperatures.

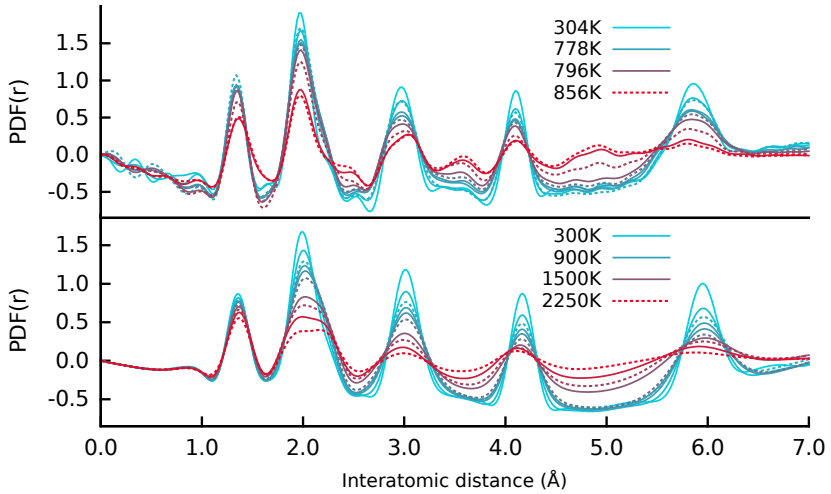

Supplementary Figure 2. Low-r region of the X-ray total pair distribution functions at different temperatures. Upper plot shows data measured on heating the ZIF-4 glass, lower plot from the partial radial distribution functions, $g_{ij}(r)$, determined from the FPMD simulation and combined to mimic the experimental data accurately.

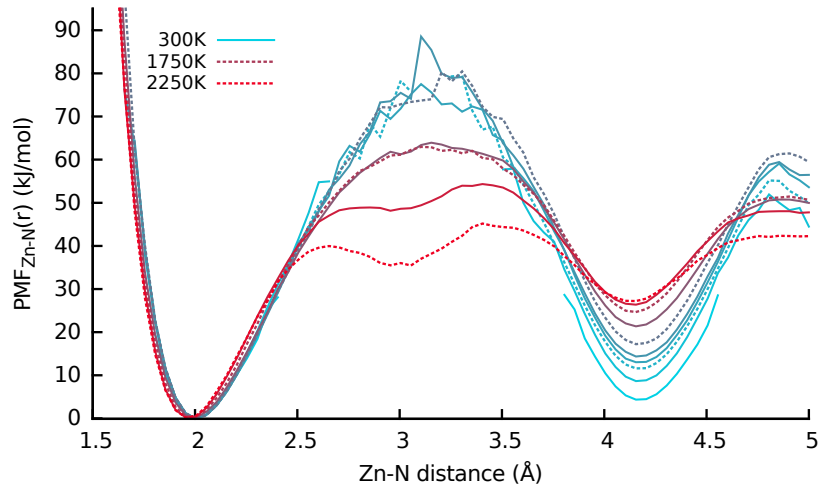

Supplementary Figure 3. Potential of mean force along the nitrogen–zinc distance coordinate at different temperatures. An activation free energy barrier can be computed from each PMF higher than 800 K.

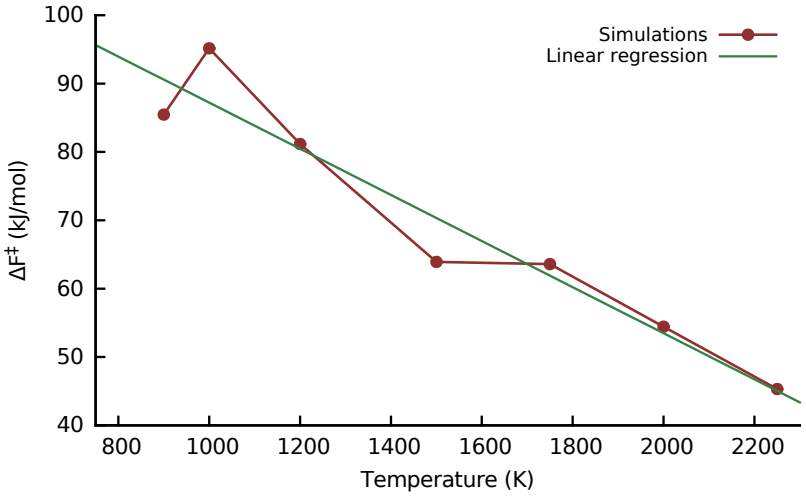

Supplementary Figure 4. Linear fit of the activation free energy. The activation free energy for breaking a Zn–N bond follows a van 't Hoff law well, with $\Delta H = 121\,\mathrm{kJ.mol^{-1}}$ and $\Delta S = 34\,\mathrm{J.mol^{-1}.K^{-1}}$.

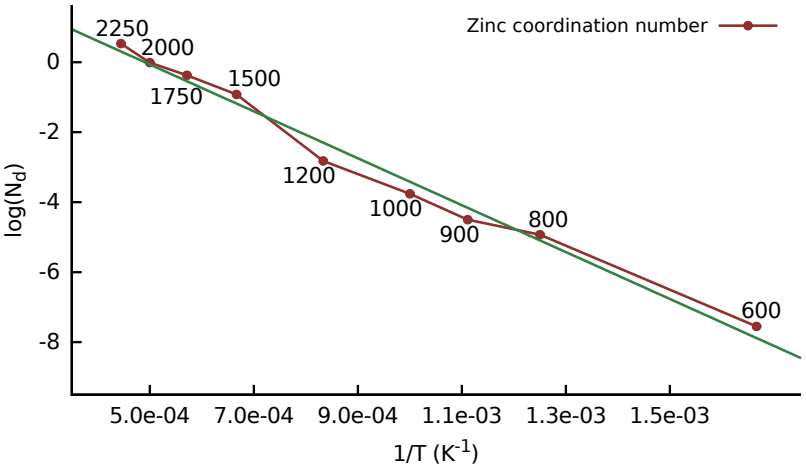

Supplementary Figure 5. van 't Hoff plot of the number of defects. The formation of defects follows an Arrhenius law associated with an activation energy of 56 kJ/mol.

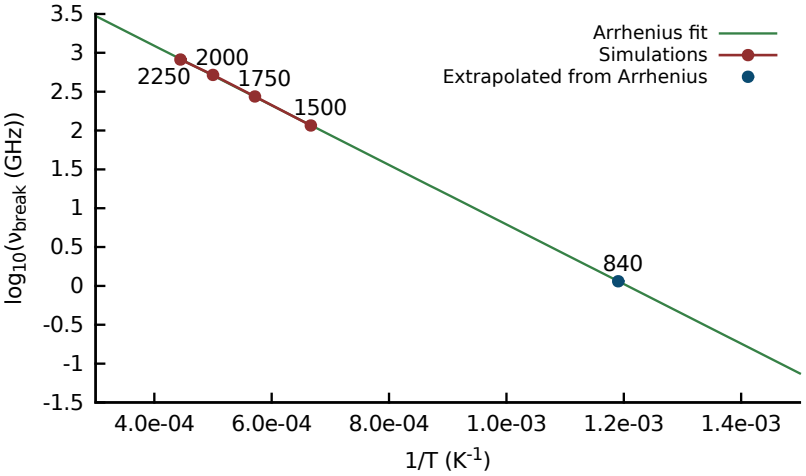

Supplementary Figure 6. Frequency of Zn–N bond breaking.

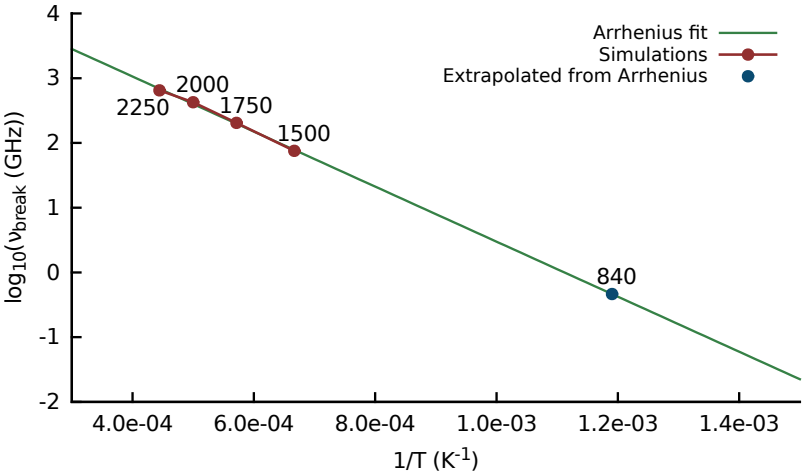

Supplementary Figure 7. Frequency of Zn–Im bond breaking.

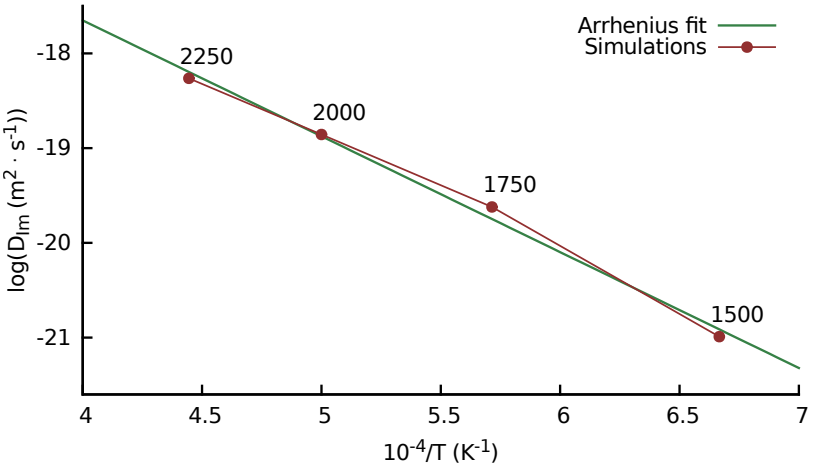

Supplementary Figure 8. van 't Hoff plot of Imidazolate diffusion coefficient.

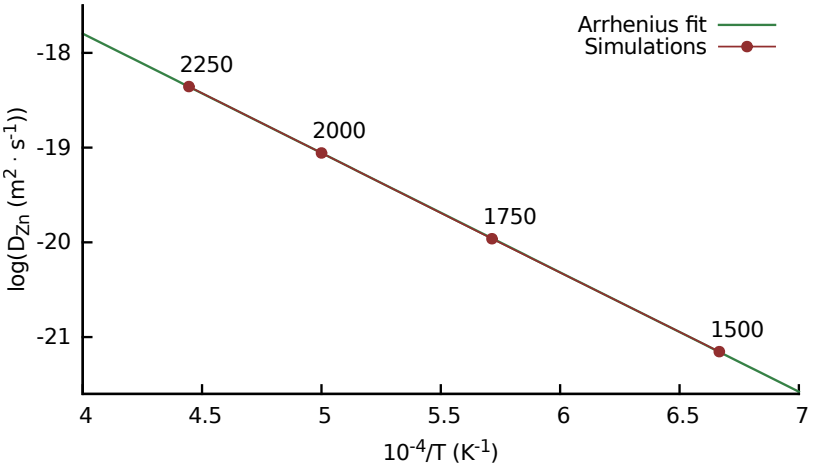

Supplementary Figure 9. van 't Hoff plot of Zinc diffusion coefficient.

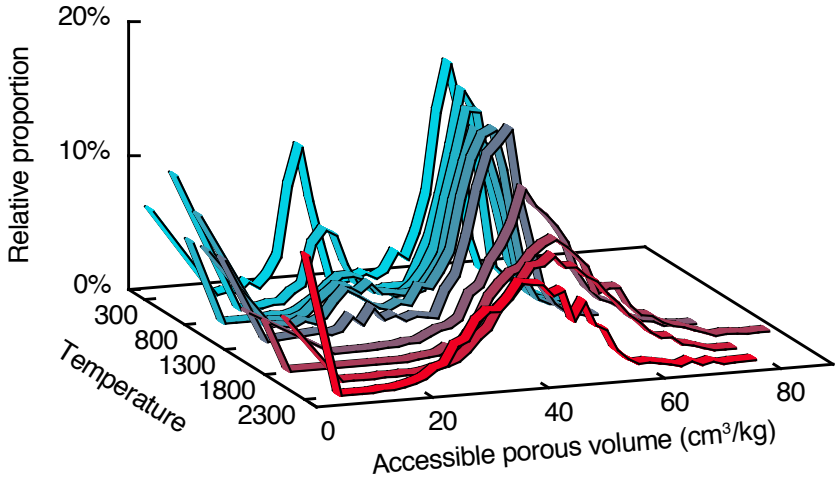

Supplementary Figure 10. Temperature evolution of the distribution of the accessible pore volume, determined for a standard probe of radius 1.2 Å.

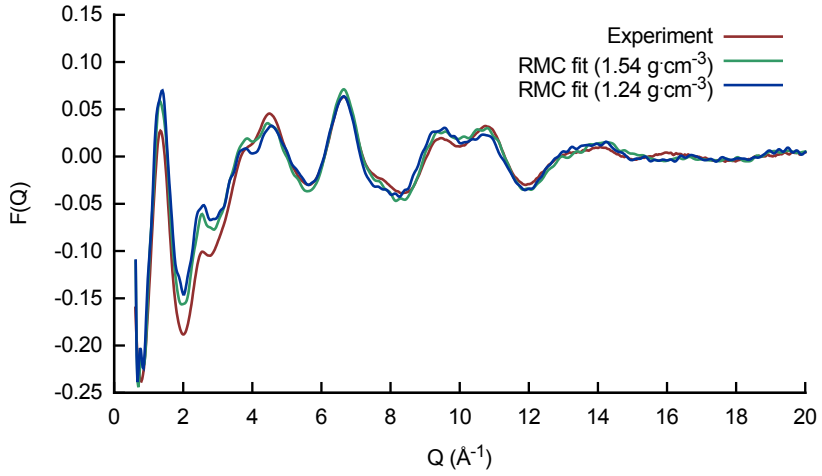

Supplementary Figure 11. Experimental X-ray structure factor data for the ZIF melt, and the fit from the configuration obtained by Reverse Monte Carlo (RMC) refinement. For comparison, we also show the fit obtained for RMC refinement at the density of 1.24 g.cm^{-3}, used in FPMD simulations.

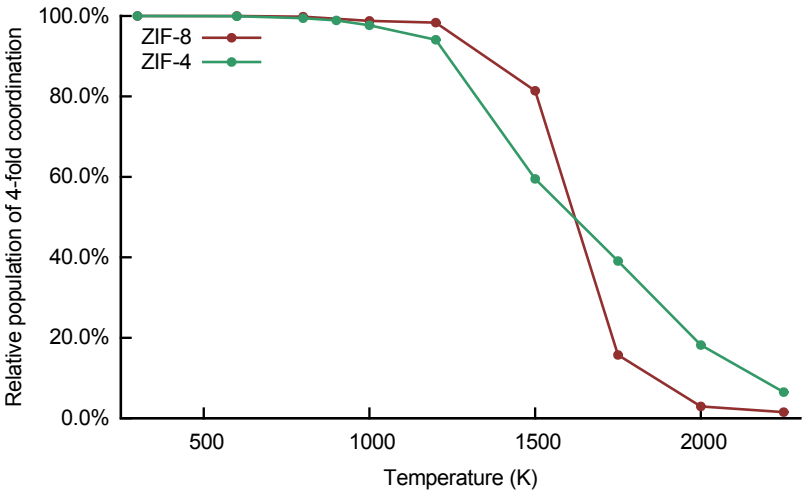

Supplementary Figure 12. Proportion of Zn^{2+} cations with four-fold coordination, as a function of temperature, for ZIF-4 and ZIF-8.

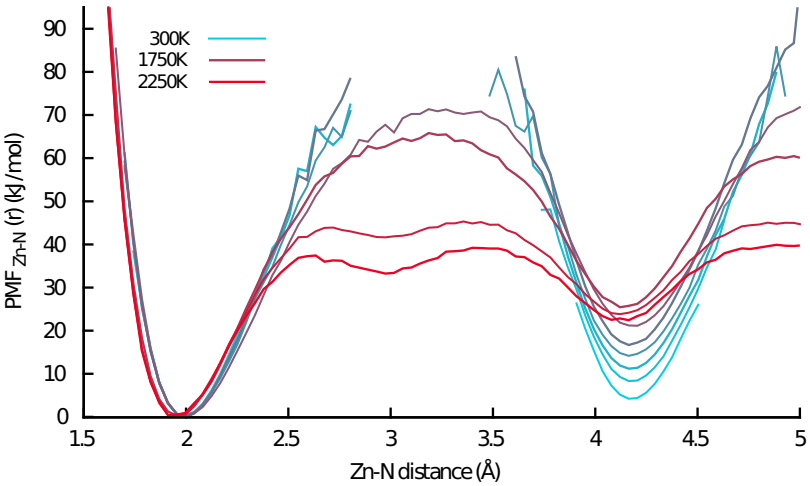

Supplementary Figure 13. Potential of mean force for ZIF-8, along the nitrogen–zinc distance coordinate, at different temperatures.

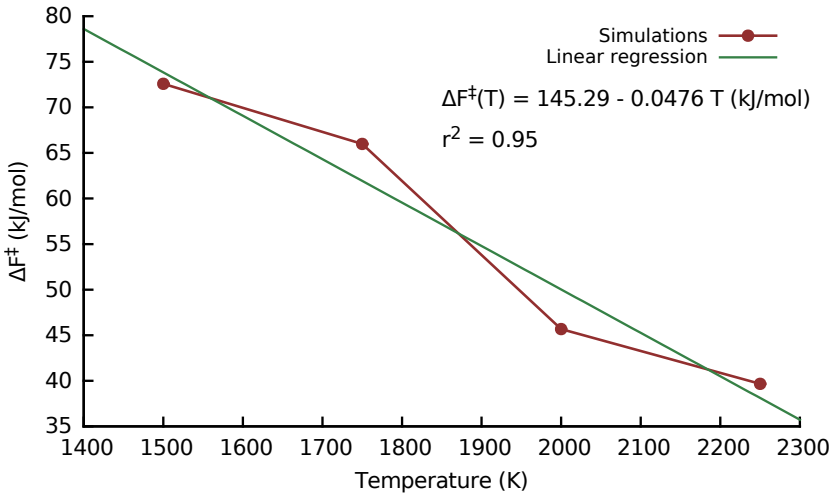

Supplementary Figure 14. Activation free energy for ZIF-8 as a function of temperature. The activation free energy for breaking a Zn–N bond is fitted by a van 't Hoff law, with $\Delta H = 145\,\mathrm{kJ.mol^{-1}}$ and $\Delta S = 48\,\mathrm{J.mol^{-1}.K^{-1}}$.

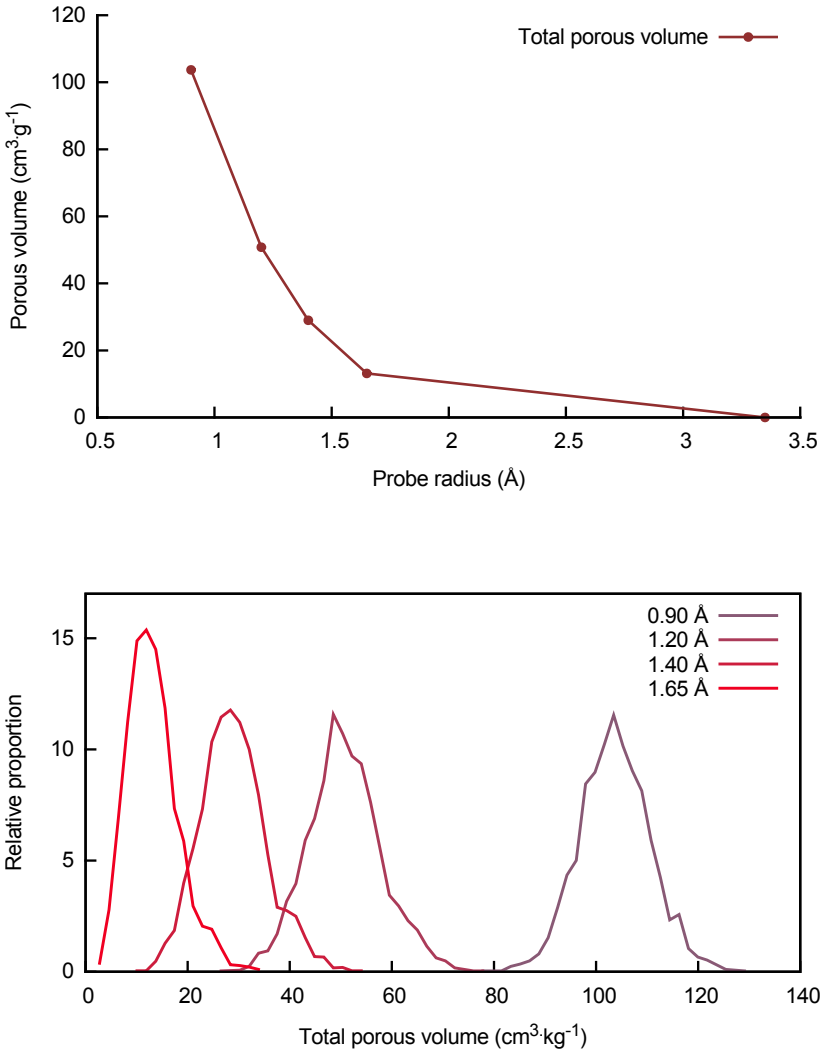

Supplementary Figure 15. Pore volume as a function of probe radius. Top: evolution of the average pore volume in molten ZIF-4 from FPMD simulations at 1,500 K, as a function of probe radius. Bottom: Distribution of instantaneous pore volume at 1,500 K, for probes of radius 0.90 Å, 1.20 Å, 1.40 Å, and 1.65 Å.

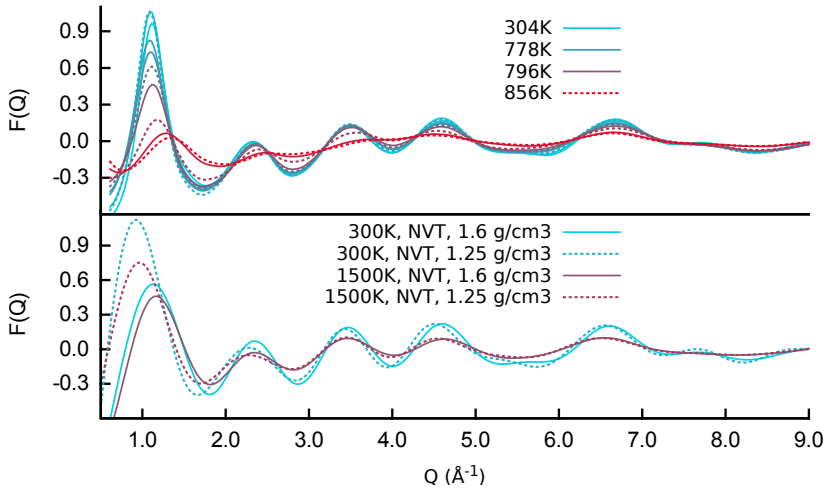

Supplementary Figure 16. X-ray structure factors upon heating. Top: experimental glass data. Bottom: computational ZIF-4, showing the effect of changes in simulation density, which affect and shift the first peak but do not overall change the evolution upon heating.

	$\Delta U^{\ddagger}(\mathrm{kJ.mol^{-1}})$	$\Delta S^{\ddagger}(\mathrm{J.mol^{-1}.K^{-1}})$	$\Delta F^{\ddagger}(840K)(\mathrm{kJ.mol^{-1}})$
Zn–N	127	37	95 ($\simeq 14kT$)
Zn–Im	128	40	95 ($\simeq 14kT$)

Supplementary Table 1. Thermodynamic properties values. The first column shows the activation enthalpy associated with a bond cleavage, the second column shows the activation entropy and the third column shows the extrapolated activation free energy at the experimental melting temperature of 840 K.

T (K)	1 Zn–N cleavage/Zn every	1 Zn–Im cleavage/Zn every	%(Im flip) in Zn–N cleavages
300	143 ms	2.8 s	95%
600	58 ns	228 ns	75%
840	0.87 ns	2.2 ns	60%

Supplementary Table 2. Characteristics of coordinative bond breaking. Columns 2 and 3 give average times for one Zn–N (respectively Zn–Im) cleavage per Zn atom.

T (K)	$\Delta t^{\text{cleav}}_{\text{Zn-N}}$(fs)	$\Delta t^{\text{form}}_{\text{Zn-N}}$(fs)	$\Delta t^{\text{cleav}}_{\text{Zn-Im}}$(fs)	$\Delta t^{\text{form}}_{\text{Zn-Im}}$(fs)	%(Im flip) in Zn–N cleavages
1,500	336	330	866	894	33%
1,750	303	322	732	768	27%
2,000	393	374	713	720	22%
2,250	418	426	669	675	17%

Supplementary Table 3. Coordinative bond breaking dynamics. The duration of the actual cleavages and reforming of bonds are rather constant and independent of temperature. We also show the observed percentage of Zn–N bond cleavages that correspond to a flip of the Im linker (rather than Zn–Im bond cleavage).

Temperature (K)	D_{Im} ($m^2.s^{-1}$)	D_{Zn} ($m^2.s^{-1}$)
1,500	$7.7\ 10^{-10}$	$6.5\ 10^{-10}$
1,750	$3.0\ 10^{-9}$	$2.1\ 10^{-9}$
2,000	$6.5\ 10^{-9}$	$5.3\ 10^{-9}$
2,250	$1.2\ 10^{-8}$	$1.1\ 10^{-8}$

Supplementary Table 4. Diffusion coefficients extracted from the MD simulations.

Method	Temperatures	Density
RMC modeling	300 K	1.625 g.cm^{-3}
RMC modeling	856 K	1.54 g.cm^{-3}
FPMD simulations	all temperatures	1.25 g.cm^{-3}

Supplementary Table 5. Summary of the densities used for RMC modeling and FPMD simulations. We also performed RMC refinement of the melt at 1.24 g.cm^{-3}, and FPMD simulations at 1.60 g.cm^{-3} (300 and 1500 K).